Calculation of resonant second-order Raman efficiencies for allowed and forbidden scattering

R. Zeyher
Max-Planck-Institut für Festkörperforschung, 7 Stuttgart 1, Bundesrepublik Deutschland
(Received 30 July 1973)

The frequency dependence of the cross section for second-order Raman scattering in an insulator is evaluated for incident frequencies below and above the gap. We consider both a deformation potential and the Fröhlich interaction for the electron-one-phonon coupling and take the uncorrelated electron-hole continuum as intermediate states. The following results compare well with recent experiments in GaP: (a) the frequency dependence of the scattering intensity with TO(Γ) + LO(Γ) and 2LO(Γ) phonons around the gap; (b) the corresponding selection rules; (c) absolute numbers for the deformation potential and the prefactor of the Fröhlich interaction using measured intensity ratios with TO(Γ) first-order scattering and a pseudopotential calculation. Calculated line shifts and widths due to phonon dispersion show a strong dependence on the incident frequency around the gap.

I. INTRODUCTION

Detailed calculations for resonant Raman efficiencies as a function of the incident frequency have been made mostly only for first-order scattering.[1-4] Theoretical investigations of second-order scattering are rather sparse. References 5 and 6 give formal expressions for the scattering amplitude for deformation-potential scattering. In Ref. 7 scattering via the electron–two-phonon interaction is discussed quantitatively and compared with experiment. The cross section for 2LO scattering has been calculated by Hamilton[8] using the Fröhlich interaction. The latter paper has been criticized[4] and its theoretical predictions are in strong disagreement with experiment (compare for instance Fig. 2 in Ref. 8 and Fig. 11 in Ref. 7).

Second-order scattering has some advantages compared to first-order scattering. The momentum selection rule says only $\vec{Q}_1 + \vec{Q}_2 \approx 0$ for the momenta of the two phonons and one has one nontrivial $\vec{Q}$ integration over final phonon states. Therefore the whole electron-phonon coupling enters and its $\vec{Q}$ dependence is reflected in the line shapes of scattered photons. Measured scattering-intensity ratios with a first-order line allow a determination of absolute values of the coupling functions. The magnitude of different contributions to the cross section can then be determined directly. From a theoretical point of view second-order scattering expressions are still simple enough to be evaluated without additional assumptions. This allows a check of the phenomenological theory of multiphonon scattering of Ref. 9. According to that theory the second-order cross section should be $\sim g$ (g is the electron-phonon coupling constant) in the frequency range $2\hbar\Omega_{LO} < \hbar\omega - E_g < 3\hbar\Omega_{LO}$. Perturbation theory would suggest a dependence $\sim g^2$ everywhere. As a necessary consequence the perturbation expression for second-order scatterng must be divergent in that frequency region.

To investigate second-order scattering we chose a two-band model with parabolic bands and free electron-hole pairs as excited states. (For simplicity, in what follows, free electron-hole pairs are also called excitons.) This model is appropriate for crystals like GaP if the spin-orbit splitting can be neglected and the degeneracy of the valence bands is taken into account by suitable averages. The different experimental resonance behavior of the cross section for 2LO(Γ), TO(Γ) + LO(Γ), 2LO(Σ), etc., phonons suggests that three different electron-phonon couplings should be considered: (a) the $\vec{Q}$-dependent intraband Fröhlich coupling; (b) a $\vec{Q}$-independent deformation potential for electron–one-phonon coupling; and (c) a $\vec{Q}$-independent deformation potential for electron–two-phonon coupling. Interaction (a) is the strongest one in GaP and couples only LO(Γ) phonons to excitons. It should be responsible for the sharp combination peaks 2LO(Γ) and LO(Γ) + TO(Γ). All other peaks are due to interactions (b) and (c). The cases (a) and (b) will be treated in this paper; case (c) has been discussed in Ref. 7. We consider only lowest-order contibutions in the photon-exciton interaction ("bare-exciton approach"). The discussions in Refs. 4 and 7 [diagrams (c) of Fig. 1 in that paper] suggest that higher-order contributions ("polariton approach") are small.

II. EVALUATION OF THE RAMAN CROSS SECTION

We split the total Hamiltonian H in H_0 and H':

$$H = H_0 + H' . \tag{1}$$

H_0 contains the free photon, exciton, and phonon

field:

$$H_0=\sum_{\vec{k}}\hbar c|\vec{k}|\,(a^\dagger_{\vec{k}}a_{\vec{k}}+\tfrac{1}{2})+\sum_{\vec{q},\vec{k}}\hbar\omega_{\vec{q}}(\vec{k})(b^\dagger_{\vec{q}\,\vec{k}}b_{\vec{q}\,\vec{k}}+\tfrac{1}{2})$$
$$+\sum_{\vec{Q},j}\hbar\Omega_j(\vec{Q})(c^\dagger_{\vec{Q}j}c_{\vec{Q}j}+\tfrac{1}{2})\,. \qquad (2)$$

$a^\dagger_{\vec{k}}$, $b^\dagger_{\vec{q}\vec{k}}$, $c^\dagger_{\vec{Q}j}$ are creation operators for photon, exciton, and phonons, respectively. $\vec{k}$ and $\vec{Q}$ denote total momenta, $\vec{q}$ the internal momentum for the relative motion of electron and hole, and j is a branch index. We omit in this section a photon polarization index for simplicity. H' contains the photon-exciton and the exciton-phonon interactions:

$$H'=\frac{ie}{m}\langle p\rangle\sum_{\vec{k},\vec{q}}\left(\frac{2\pi\hbar}{c|\vec{k}|}\right)^{1/2}b_{\vec{q}\vec{k}}(a^\dagger_{\vec{k}}+a_{-\vec{k}})+\text{c.c.}$$
$$+\sum_{\vec{k}}\frac{\omega_p^2}{|\vec{k}|}\frac{\hbar}{4c}(a^\dagger_{\vec{k}}+a_{-\vec{k}})(a^\dagger_{-\vec{k}}+a_{\vec{k}})$$
$$+\sum_{\substack{\vec{q},\vec{q}',\vec{k}\\ \vec{Q},j}}f_{\vec{q},\vec{q}'}(\vec{Q},j)b^\dagger_{\vec{q}\vec{k}}b_{\vec{q}',\vec{k}+\vec{Q}}c^\dagger_{\vec{Q}j}+\text{c.c.} \qquad (3)$$

m is the electron mass and $\langle p\rangle$ the momentum matrix element between the two bands. Explicit expressions for the coupling function $f_{\vec{q},\vec{q}'}(\vec{Q},j)$ are[3]

$$f_{\vec{q},\vec{q}'}(\vec{Q},j)=\int d\vec{r}\,\varphi^*_{\vec{q}}(\vec{r})f_{\vec{Q}j}(\vec{r})\varphi_{\vec{q}'}(\vec{r}) \qquad (4)$$

with

$$f_{\vec{Q}j}(\vec{r})=-C\left(\frac{a^3}{V}\right)^{1/2}e^{-is_h\vec{Q}\cdot\vec{r}}\,, \qquad (5)$$

or

$$f_{\vec{Q}j}(\vec{r})=(C_F/|\vec{Q}|)(e^{is_e\vec{Q}\cdot\vec{r}}-e^{-is_h\vec{Q}\cdot\vec{r}})\,, \qquad (6)$$

$$C_F=i\delta_{j,\mathrm{LO}}\hbar\Omega_{\mathrm{LO}}\left(\frac{\hbar}{2\mu\Omega_{\mathrm{LO}}}\right)^{1/4}\left(\frac{4\pi\alpha}{V}\right)^{1/2}, \qquad (7)$$

$$\alpha=\frac{e^2}{\hbar}\left(\frac{1}{\epsilon_\infty}-\frac{1}{\epsilon_0}\right)\left(\frac{\mu}{2\hbar\,\Omega_{\mathrm{LO}}}\right)^{1/2}. \qquad (8)$$

m denotes the reduced mass, a is a reference length defined by $\hbar^2/2\mu a^2=\hbar\Omega_{\mathrm{LO}}$, Ω_{LO} is the longitudinal-optical frequency at $\vec{q}=0$, V is the crystal volume, and $s_e=m_h/M$, $s_h=m_e/M$, where M is the total exciton mass. $\varphi_{\vec{q}}(\vec{r})$ is the wave function for the relative motion of the electron and hole. Equation (5) describes a deformation-potential coupling for optical phonons with the constant C, Eq. (6) the intraband Frölich coupling.

The cross section for fixed final branch indices j_1, j_2 is given by

$$\frac{d\sigma}{d\Omega}=\frac{2\pi}{\hbar c}\sum_{\vec{k}_0',\vec{Q}}|\langle f|T(\omega+i\eta)|i\rangle|^2$$
$$\times\delta(\hbar\omega-\hbar\omega'-\hbar\Omega_{j_1}(\vec{Q})-\hbar\Omega_{j_2}(-\vec{Q}))\,. \qquad (9)$$

The initial state $|i\rangle$ is

$$|i\rangle=a^\dagger_{\vec{k}_0}|0\rangle\,, \qquad (10)$$

the final state $|f\rangle$ is

$$|f\rangle=a^\dagger_{\vec{k}_0'}c^\dagger_{\vec{Q}j_1}c^\dagger_{-\vec{Q}j_2}|0\rangle\,. \qquad (11)$$

The collision operator T is

$$T(z)=H'+H'\frac{1}{z-H}H'$$
$$=H'+H'\frac{1}{z-H_0}H'+H'\frac{1}{z-H_0}H'\frac{1}{z-H_0}H'+\cdots. \qquad (12)$$

In lowest-order perturbation theory the last term in the expansion (12) must be taken. The sum over intermediate states can be carried out by using the explicit expression for the free-electron Green's function:

$$\sum_{\vec{q}}\frac{\varphi_{\vec{q}}(\vec{r})\varphi^*_{\vec{q}}(\vec{r}')}{\hbar\omega+i\eta-\hbar^2q^2/2\mu}=\frac{1}{a^2\hbar\Omega_{\mathrm{LO}}}\frac{e^{ik|\vec{r}-\vec{r}'|}}{4\pi|\vec{r}-\vec{r}'|}\,, \qquad (13)$$

with

$$\hbar^2k^2/2\mu=\hbar\omega+i\eta-E_g\,,\quad \mathrm{Im}k>0\,.$$

Using Eq. (13) the cross section (9) becomes

$$\frac{d\sigma}{d\Omega}=k_0'^3k_0\frac{2e^4|\langle p\rangle|^4V^2}{m^4\omega^2\omega'^2(\hbar\Omega_{\mathrm{LO}})^2a^{12}(4\pi)^6}\sum_{\vec{Q}}\left|\int d\vec{r}\,d\vec{r}'\right.$$
$$\times\frac{e^{ik_1r}}{r}f_{\vec{Q}j_1}(\vec{r})\frac{1}{|\vec{r}-\vec{r}'|}e^{ik_2|\vec{r}-\vec{r}'|}\frac{e^{ik_3r'}}{r'}$$
$$\left.\times f_{-\vec{Q}j_2}(\vec{r}')\right|^2; \qquad (14)$$

k_i is defined by

$$\hbar^2k_i^2/2\mu=\hbar\omega+i\eta-E_g-(i-1)\hbar\Omega-\delta_{i_2}\hbar^2Q^2/2M\,. \qquad (15)$$

If $j_1\neq j_2$ an additional term with j_1, j_2 interchanged must be added inside the brackets in Eq. (14) and the total expression multiplied by 0.5.

The main problem left is the evaluation of the integral

$$A(\lambda_1\vec{q},\lambda_2\vec{q},k_1,k_2,k_3)=\int d\vec{r}\,d\vec{r}'\frac{e^{ik_1r}}{r}e^{i\lambda_1\vec{q}\cdot\vec{r}}$$
$$\times\frac{e^{ik_2|\vec{r}-\vec{r}'|}}{|\vec{r}-\vec{r}'|}\frac{e^{ik_3r'}}{r'}e^{i\lambda_2\vec{q}\cdot\vec{r}'}\,. \qquad (16)$$

We consider first the case $\lambda_1=0$. Introducing ellipsoidal coordinates for the $\vec{r}$ integration

$$r=\tfrac{1}{2}r'(\xi+\eta),\qquad |\vec{r}-\vec{r}'|=\tfrac{1}{2}r'(\xi-\eta)\,,$$
$$d\vec{r}=(\tfrac{1}{2}r')^3(\xi^2-\eta^2)\,,\quad -1<\eta<1,\ 1<\xi<\infty$$

we obtain after carrying out the $\vec{r}$ integration

$$\frac{4\pi}{(k_1^2-k_2^2)}\int d\vec{r}'\,\frac{1}{r'^2}e^{ik_3r'}e^{i\lambda_2\vec{q}\cdot\vec{r}'}(e^{ik_1r'}-e^{ik_2r'})\,. \qquad (17)$$

The $\vec{r}'$ integration can be done in polar coordinates

and one obtains

$$A(0, \lambda_2\vec{q}, k_1, k_2, k_3) = \frac{16\pi^2}{(k_1^2 - k_2^2)\lambda_2 |\vec{q}|}\left[\arctan\left(\frac{i\lambda_2 q}{k_1 + k_3}\right) - \arctan\left(\frac{i\lambda_2 q}{k_2 + k_3}\right)\right]. \quad (18)$$

From the definition (16) follow moreover the relations

$$A(\vec{q}, 0, k_1, k_2, k_3) = A(0, \vec{q}, k_3, k_2, k_1) ,$$
$$A(\vec{q}, -\vec{q}, k_1, k_2, k_3) = A(0, \vec{q}, k_1, k_3, k_2) . \quad (19)$$

The general case $\lambda_1 \neq -\lambda_2$ can be reduced to the case $\lambda_1 = 0$. To show that we observe that

$$\frac{e^{ik_2 r}}{r} = 4\pi \int \frac{d\vec{q}\,'}{(2\pi)^3} \frac{e^{i\vec{q}'\cdot\vec{r}}}{q'^2 - k_2^2} . \quad (20)$$

Inserting (20) into (16) and carrying out the $\vec{r}$ and $\vec{r}\,'$ integrations in polar coordinates we obtain

$$A(\lambda_1\vec{q}, \lambda_2\vec{q}, k_1, k_2, k_3) = -8 \int d\vec{q}\,' \frac{1}{(q'^2 - k_2^2)} \times \frac{1}{k_1^2 - (\lambda_1\vec{q} + \vec{q}\,')^2} \frac{1}{k_3^2 - (\lambda_2\vec{q} - \vec{q}\,')^2} . \quad (21)$$

One easily verifies that

$$\frac{1}{k_1^2 - (\lambda_1\vec{q} + \vec{q}\,')^2} \frac{1}{k_3^2 - (\lambda_2\vec{q} - \vec{q}\,')^2} = \frac{1}{\lambda_1 + \lambda_2} \times \left(\frac{\lambda_1}{(S - q'^2)[k_1^2 - (\lambda_1\vec{q} + \vec{q}\,')^2]} + \frac{\lambda_2}{(S - q'^2)[k_3^2 - (\lambda_2\vec{q} - \vec{q}\,')^2]}\right), \quad (22)$$

with

$$S = \frac{\lambda_1 k_3^2 + \lambda_2 k_1^2}{\lambda_1 + \lambda_2} - \lambda_1\lambda_2 q^2 . \quad (23)$$

Comparison of Eq. (21) and Eq. (22) yields

$$A(\lambda_1\vec{q}, \lambda_2\vec{q}, k_1, k_2, k_3) = \frac{\lambda_1}{\lambda_1 + \lambda_2} A(0, \lambda_1\vec{q}, S^{1/2}, k_2, k_1) + \frac{\lambda_2}{\lambda_1 + \lambda_2} A(0, \lambda_2\vec{q}, S^{1/2}, k_2, k_3) . \quad (24)$$

Denoting the iterated deformation process by 2TO, the mixed deformation potential and Fröhlich case by TO + LO, and the iterated Fröhlich case with 2LO, we obtain the following three possibilities for the second-order cross section:

$$\frac{d\sigma^{2\mathrm{TO}}}{d\Omega} = F \int_0^\infty dx\; x^2 |A(s_h x, -s_h x, x_1, x_2, x_3)|^2 , \quad (25)$$

$$\frac{d\sigma^{\mathrm{TO+LO}}}{d\Omega} = \frac{F}{2}\left(\frac{C_F a}{C}\right)^2 \int_0^\infty dx\, |A(s_h, s_e x, x_1, x_2, x_3) - A(-s_h x, s_h x, x_1, x_2, x_3) + A(s_h x, s_e x, x_3, x_2, x_1) - A(-s_h x, s_h x, x_3, x_2, x_1)|^2 , \quad (26)$$

$$\frac{d\sigma^{2\mathrm{LO}}}{d\Omega} = F\left(\frac{C_F a}{C}\right)^4 \int_0^\infty \frac{dx}{x^2} |A(s_e x, -s_e x, x_1, x_2, x_3) + A(s_h x, -s_h x, x_1, x_2, x_3) - A(s_e x, s_h x, x_1, x_2, x_3) - A(s_h x, s_e x, x_1, x_2, x_3)|^2 . \quad (27)$$

F is a prefactor and has the dimension of an area:

$$F = \frac{k_0'^3 k_0 e^4 |\langle p\rangle|^4 V C^4}{m^4\omega^2\omega'^2(\hbar\Omega_{\mathrm{LO}})^6 a^3\pi^2(4\pi)^6} , \quad (28)$$

x, x_1, x_2, x_3 are dimensionless momenta $x = aQ$, $x_i = ak_i$.

III. DISCUSSION AND COMPARISON WITH EXPERIMENT

A. Convergence properties of the cross section in the limit $\eta \to 0$

The integrals in Eqs. (25)–(27) converge for finite $\eta > 0$. Using Eqs. (18), (19), and (24) it is straightforward to show that all integrals converge also in the limit $\eta \to 0$ which corresponds to lowest-order perturbation theory. As a consequence the cross section is proportional to the fourth power of the electron-phonon coupling constants C or C_F for all four possibilities.

This result disagrees with the phenomenological cascade theory of Ref. 9. In the cascade theory it is assumed that the leading terms in the cross section Eq. (9) are obtained by taking as many energy-conserving steps (that is, the imaginary parts of the energy denominators) as possible. Momentum conservation causes at least one virtual step and correspondingly the leading terms of Eq. (9) should be proportional to the square of C or C_F for incident frequencies in the electron-hole continuum. The discrepancy to our results can be traced back[10] to the fact that Ref. 9 did not take into account all possible arrangements for the virtual step and also neglected interference terms between different decay channels.

Recently Yu *et al.* reported a $1/\eta$ behavior of the cross section in Cu_2O.[11] For incident frequencies below the phonon-assisted $1s$ threshold ($\omega \leq \omega_{1s} + \Omega$, ω_{1s} is the forbidden $1s$ exciton of the yellow series, Ω the Γ_{12}^- phonon), the cross section is very small. Above the threshold ($\omega > \omega_{1s} + \Omega$) it is proportional to $(\omega - \omega_{1s} - \Omega)^{1/2}/\eta$ [correcting a print error in Eq. (7) in that reference] and therefore divergent in the limit $\eta \to 0$. The difference to our results comes from the fact that Ref. 11 uses a discrete exciton band while we deal with the electron-hole continuum and integrate over the continuous internal quantum number of the excitons. Correspondingly the $1/\eta$ singularity of Ref. 11 is smeared out leading to a cross section which is regular for $\eta \to 0$.

A numerical evaluation of the 2LO cross section

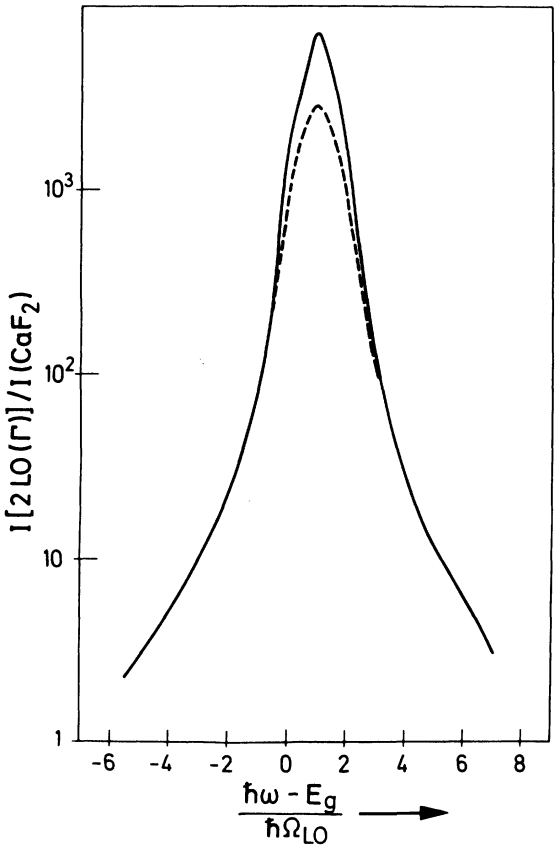

FIG. 1. Theoretical cross section $I(2\mathrm{LO}(\Gamma))$ for 2LO (Γ) scattering for two different exciton dampings: Straight line calculated with $0.1\hbar\Omega_{\mathrm{LO}}$; dashed line with $0.3\hbar\Omega_{\mathrm{LO}}$. The curves were obtained by evaluating Eq. (27).

shows that the maximum in the enhancement curve which occurs at about $\omega = E_g/\hbar + \Omega_{\mathrm{LO}}$ depends sensitively on exciton damping. This is shown in Fig. 1 where two dampings $\eta = 0.1\hbar\Omega_{\mathrm{LO}}$ and $0.3\hbar\Omega_{\mathrm{LO}}$ have been used in evaluating Eq. (27). The behavior of the TO + LO cross section for different exciton dampings is similar. In this case the maximum occurs at about $\omega = E_g/\hbar + 2\Omega_{\mathrm{LO}}$ and increases by a factor of 3 if the damping is reduced from $0.3\hbar\Omega_{\mathrm{LO}}$ to $0.1\hbar\Omega_{\mathrm{LO}}$.

B. Frequency dependence of the cross sections

As discussed in Sec. III A the theoretical cross sections depend sensitively on exciton damping if the frequency of the scattered photons is near the band edge. Every comparison with experimental data based on temperature tuning of the gap is therefore difficult. In the following we use experimental points of Ref. 7 which were obtained by varying the temperature between 77 and 670 °K. To be able to make a comparison of theory and experiment at all we chose a constant exciton damping η of $0.3\hbar\Omega_{\mathrm{LO}}$. This value reproduces the high-frequency decrease of 2LO scattering quite well.

The solid line in Fig. 2 shows the frequency dependence of iterated deformation-potential scattering, Eq. (25), using the damping $0.3\hbar\Omega_{\mathrm{LO}}$ and the phonon frequency Ω_{TO} with $\Omega_{\mathrm{TO}}/\Omega_{\mathrm{LO}} = 0.91$ appropriate for GaP. The broken line shows the frequency dependence of the corresponding first-order deformation-potential scattering. Below the gap the increase of the two curves is similar, though the second-order scattering expression originally had one energy denominator more. This additional denominator contains the phonon momentum in the kinetic energy of the scattered exciton and therefore takes part in the momentum integration over final phonon states. As a result this additional energy denominator increases the resonance enhancement only weakly below the gap. The maximum of the solid line occurs about at $\omega = (E_g + 2\hbar\Omega_{\mathrm{TO}})/\hbar$, that of the broken line at $\omega = (E_g + \frac{1}{2}\hbar\Omega_{\mathrm{TO}})/\hbar$. The solid line shows also that the cross section (25) is no longer symmetric with respect to the frequency where the scattering maximum occurs like the first-order cross section. Instead the scattering intensity is substantially enhanced in the continuum.

The integrand in Eq. (25) decreases $\sim 1/x^2$ with

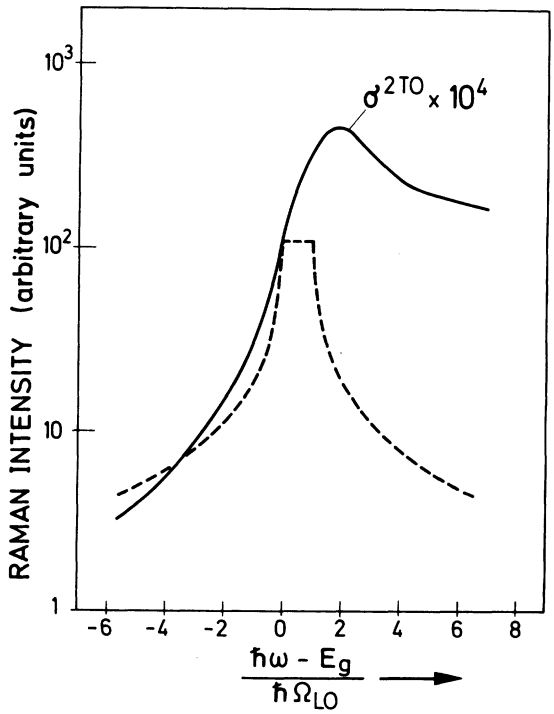

FIG. 2. Solid line: Raman intensity for iterated deformation-potential scattering, Eq. (25), using $\eta = 0.1\hbar\Omega_{\mathrm{LO}}$ and the transversal-phonon frequency Ω_{TO} with $\Omega_{\mathrm{TO}}/\Omega_{\mathrm{LO}} = 0.91$ for GaP. Broken line: First-order Raman intensity for TO(Γ) scattering in GaP.

increasing momentum. The decrease should be slower for incident frequencies below the gap because the increase in the kinetic energy with momentum is not very effective owing to the presence of the other summand $\hbar\omega - E_g$ in x_2. Indeed, the numerical calculation shows that substantial contributions to the integral come from all parts in the Brillouin zone for $\hbar\omega - E_g < 0$. This means that an adequate theoretical description needs realistic electron and phonon dispersion curves throughout the Brillouin zone. By introducing a suitable cutoff one can limit the final two phonon states to what could be described as a 2TO(Γ) peak. The area under this peak would increase somewhat steeper than the solid line in Fig. 2 below the gap. The situation is much simpler for incident frequencies above the gap: The dominant contribution to the integral comes from a very small region around the zone center. The assumption of parabolic exciton bands and neglect of phonon dispersion is well justified in this case. Equation (25) and the solid line in Fig. 2 therefore describe 2TO(Γ) scattering for incident frequencies above the gap. The width of the peak is determined by the sharp decrease of the integrand in Eq. (25) with momentum and not by phonon densities. Using the deformation potential $C/\hbar\Omega_{LO} = 0.1$ appropriate for optical phonons at Γ in GaP (see Sec. III D) Eqs. (25) and (35) predict a theoretical ratio of about 4×10^{-4} for the maxima of 2TO(Γ) and 1TO(Γ) scattering. This number is smaller by a factor 20 than the experimental ratios of dominant two-phonon peaks (owing to zone edge phonons) and the first-order peak in GaP. This may explain why the 2TO(Γ) peak was not observed in Ref. 7.

The situation for the sharp and strongly resonating TO(Γ)+LO(Γ) and 2LO(Γ) peaks is much simpler. The $\vec{Q}$ dependence of the Fröhlich interaction allows only near-center phonons to participate. This explains the sharpness of these peaks and also justifies the use of parabolic bands and the continuum approximation in deriving the Fröhlich interaction. Figures 3 and 4 show the results of a numerical evaluation of Eqs. (26) and (27) and experimental points of Ref. 7. We shifted the experimental points towards higher frequencies by $1\hbar\Omega_{LO}$ in Fig. 3 and $0.35\hbar\Omega_{LO}$ in Fig. 4 for the comparison. The origin of these shifts is presently unclear though similar shifts occur in other crystals.[12] They could be due to the neglect of the electron-hole correlation and the presence of discrete excitons or to the neglect of the real part of the exciton self-energy. The agreement of theory and experiment is quite good.

C. Selection rules

The cross sections (25)–(27) refer to a simple two-band model. To relate these expressions to the more complicated situation in GaP we observe that the highest valence band in GaP is threefold degenerate at the Γ point if the spin-orbit interaction is neglected. The three components u_{0i} transform like the three Cartesian coordinates x_i and belong to Γ_{15}. The lowest conduction band transforms like Γ_1 and the optical phonon like Γ_{15}. The electron-phonon matrix element for deformation-potential scattering is zero for the conduction band and of the form

$$\langle u_{0i} \left| \frac{\partial V}{\partial Q_j} \right| u_{0e} \rangle \tag{31}$$

for the valence bands. The indices i and l are identical with the polarization indices and Q_j denotes one of the three components of the optical phonon. T_d symmetry implies that all three Cartesian indices in (31) must be different from each other to get a nonzero matrix element.

The Fröhlich interaction between an electron and an isotropic medium can be written as[13]

$$\sum_{\vec{Q}i} \frac{C_F}{|\vec{Q}|} e^{i\vec{Q}\cdot\vec{r}} c_{\vec{Q}}^{\dagger} + \text{c. c.}\ , \tag{32}$$

where $\vec{r}$ is the position operator of the electron.

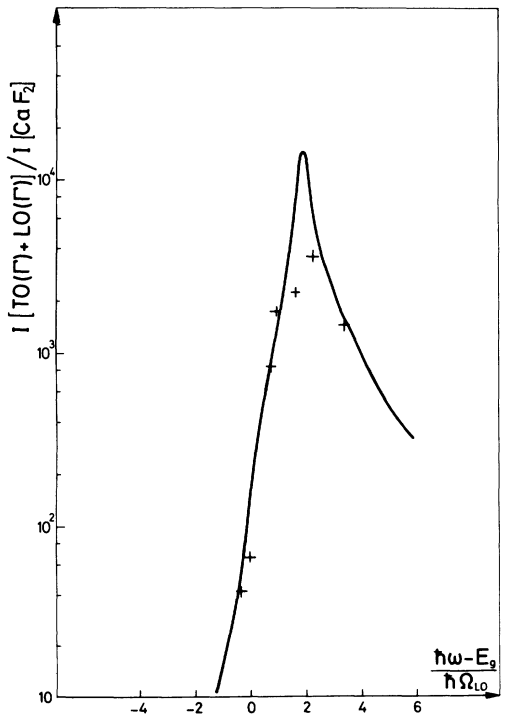

FIG. 3. Theoretical cross section for TO(Γ)+LO(Γ) scattering, Eq. (26), together with experimental points of Ref. 7. A constant damping of $0.3\hbar\Omega_{LO}$ was used. The experimental points were shifted towards higher frequencies by $1.0\Omega_{LO}$.

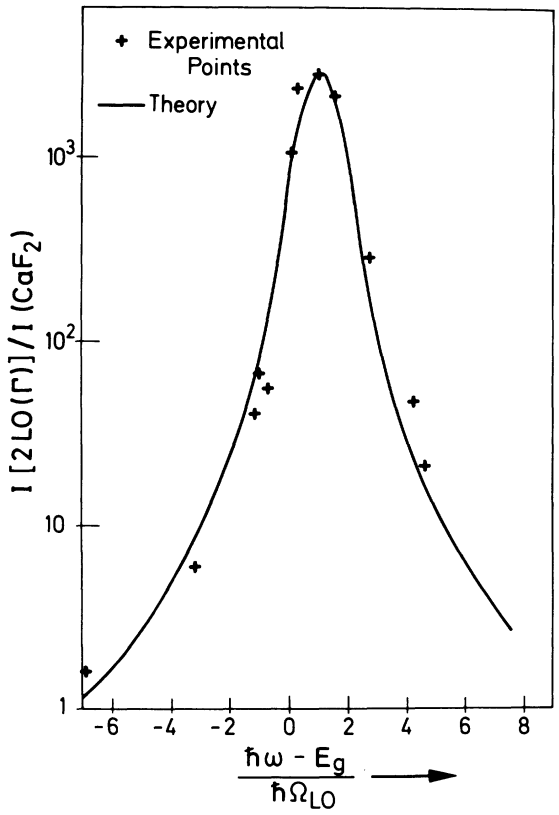

FIG. 4. Theoretical cross section for 2LO(Γ) scattering, Eq. (27), together with experimental points of Ref. 7. A constant exciton damping of $0.3\hbar\Omega_{LO}$ was used. The experimental points were shifted towards higher frequencies by $0.35\Omega_{LO}$.

Using Bloch functions $\psi_{\vec{k}j}(\vec{r})$ to form matrix elements, Eq. (32) becomes

$$\sum_{\vec{Q},\vec{k},i,j} \frac{C_F}{|\vec{Q}|} \langle \psi_{\vec{k},i} | e^{i\vec{Q}\cdot\vec{r}} | \psi_{\vec{k}+\vec{Q},j} \rangle c_{\vec{Q}}^{\dagger} \psi_{\vec{k},i}^{\dagger} \psi_{\vec{k}+\vec{Q},j} + \text{c.c.} \tag{33}$$

The matrix element in (33) is

$$\langle u_{\vec{k},i} | u_{\vec{k}+\vec{Q},j} \rangle = \delta_{ij} \tag{34}$$

neglecting the momentum dependence of the periodic part of the Bloch function. Equation (34) means that a LO phonon interacting via the Fröhlich interaction behaves in the selection rules like a Γ_1 phonon. Using Eqs. (31) and (34) the different contributions to the irreducible components Γ_1, Γ_{12}, Γ_{15} of the cross section can be worked out and are shown in Table I.[14] $I(2TO)$, $I(TO+LO)$, and $I(2LO)$ denote the expressions (25)–(27).

The last two lines in Table I can be compared with experimental data of Ref. 7 and are in excellent agreement. For instance the Γ_{12} and Γ_{15} components of 2LO(Γ) scattering are about 50 times smaller than the Γ_1 component.

D. Absolute values for the electron-phonon coupling parameters

A similar derivation as in Sec. II gives for the first-order TO(Γ) cross section

$$\frac{d\sigma^{TO}}{d\Omega} = F \frac{256\pi^6(\hbar\Omega_{LO})^3}{C^2\hbar\Omega_{TO}} \times \left| \left(\frac{\hbar\omega - E_g}{\hbar\Omega_{TO}} \right)^{1/2} - \left(\frac{\hbar\omega - E_g - \hbar\Omega_{TO}}{\hbar\Omega_{TO}} \right)^{1/2} \right|^2 . \tag{35}$$

By forming the ratio $(d\sigma^{TO+LO}/d\Omega)/(d\sigma^{TO}/d\Omega)$ and using experimental ratios from Ref. 7 the Fröhlich coupling constant aC_F can be determined. Similarly the deformation potential C can be determined from the ratio $(d\sigma^{2LO}/d\Omega)/(d\sigma^{TO}/d\Omega)$. Tables II and III give calculated values for several incident frequencies. The TO + LO and 2LO scattering cross sections were shifted like in Figs. 3 and 4 and the TO(Γ) cross section was corrected for the spin-orbit interaction.[7]

From Tables II and III we find the following average values:

$$aC_F/\hbar\Omega_{LO} = 2.42 \quad \text{and} \quad C/\hbar\Omega_{LO} = 0.22 .$$

From the deviations from the mean values in Tables II and III we expect an uncertainty of about a factor 2. Both values can be calculated in a more direct way. Equations (7) and (8) together with the experimental input of Table IV give

$$aC_F/\hbar\Omega_{LO} = 1.08 .$$

The deformation potential C has been calculated for Ge using a pseudopotential approach.[15] The value obtained was $C/\hbar\Omega_{LO} = 0.111$ (corresponding to $d_0 = 30$ eV in the nomenclature of Ref. 13), and it was suggested that similar values should also hold for comparable III-IV compounds. The Appendix generalizes this approach to GaP taking into account also the antisymmetric part of the pseudopotential. Using values for the pseudopotential from Ref. 16 we obtain for GaP $C/\hbar\Omega_{LO} = 0.097$. Both coupling coefficients determined from scattering data are too large by a factor of 2 compared with the more reliable directly calculated values. This discrepancy could easily be removed by

TABLE I. Theoretical intensities of the Raman peaks 2 TO(Γ), TO(Γ) + LO(Γ) and 2 LO(Γ) for the three irreducible symmetry components Γ_1, Γ_{12}, and Γ_{15}.

Phonons	Contribution to the component	Γ_1	Γ_{12}	Γ_{15}
2TO(Γ)		$\frac{2}{3}I(2TO)$	$\frac{1}{3}I(2TO)$	$I(2TO)$
TO(Γ) + LO(Γ)		0	0	$I(TO+LO)$
2LO(Γ)		$I(2LO)$	0	0

TABLE II. Intensity ratio of the TO(Γ) + LO(Γ) peak to the 1 TO(Γ) peak. The second column contains theoretical values, the third one is obtained by comparing the values of the second column with experimental values of Ref. 7.

$(\omega - E_g/\hbar)/\Omega_{LO}$	$I(\mathrm{TO}+\mathrm{LO})/I(\mathrm{TO})$	$aC_F/\hbar\Omega_{LO}$
−1.4	0.136×10^{-3}	1.47
−1.1	0.24×10^{-3}	1.38
−0.3	0.96×10^{-3}	2.77
−0.1	0.121×10^{-2}	3.6
0.6	0.375×10^{-2}	2.28
1.2	0.4×10^{-2}	2.95
2.35	0.202×10^{-2}	2.50

choosing a somewhat larger electron-hole mass. The large fluctuations in the values of Tables II and III due to the uncertainties in the experimental points and the not understood shifts make on the other hand an error of a factor of 2 or 3 quite plausible.

The above absolute values show that the Fröhlich constant is about 10 times larger than the deformation potential. LO(Γ) phonons couple with electrons via the Fröhlich interaction as well as via a deformation potential. Equations (23)–(25) suggest that for LO(Γ) phonons and second-order scattering the Fröhlich coupling is two orders of magnitude larger than the deformation-potential coupling assuming the integrals have the same order of magnitude. This is indeed correct. For instance in the case of TO + LO scattering the cross section for mixed deformation-potential–Fröhlich scattering is about 20 times larger than for pure deformation-potential scattering for $\hbar\omega \approx E_g + 2\hbar\Omega_{\mathrm{LO}}$. This justifies our assumption that the iterated deformation-potential process can be neglected for TO + LO and 2LO scattering.

E. Line shapes of the scattered photons due to phonon dispersion

The cross sections (25)–(27) have the form

$$\frac{d\sigma}{d\Omega} \sim \int_0^\infty dx\, I(x) \ .$$

TABLE III. Intensity ratio of the 2 LO(Γ) peak to the 1 TO(Γ) peak. The second column contains theoretical values, the third one is obtained by comparing the values of the second column with experimental values of Ref. 7.

$(\omega - E_g/\hbar)/\Omega_{LO}$	$I(2\mathrm{LO}/I(\mathrm{TO})$	$C/\hbar\Omega_{LO}$
−1.4	0.82×10^{-1}	0.194
−1.1	0.154	0.163
−0.35	0.814	0.313
−0.1	1.38	0.36
2.35	0.56	0.195
3.9	0.023	0.121

TABLE IV. Experimental constants used in the calculation. The first three values are from Ref. 17, the fifth from Ref. 18, and the fourth, describing an averaged valence-band mass, is deduced in the spirit of Ref. 15.

ϵ_0	ϵ_∞	m_e/m	m_h/m	$\hbar\Omega_{\mathrm{LO}}$ (cm^{-1})
10.2	8.47	0.13	0.39	402

The associated cross sections which are also differential in the scattered frequency are

$$\frac{d^2\sigma}{d\Omega d\omega'} \sim \int_0^\infty dx\, I(x)\delta(\hbar\omega - \hbar\omega' - \hbar\Omega_{j_1}(x) - \hbar\Omega_{j_2}(x)) \ .$$

Using a parabolic approximation for the momentum dependence of optical phonons:

$$\hbar\Omega_j(x) = \hbar\Omega_j(0) - \hbar^2x^2/2M_ja^2 \ ,$$

we obtain

$$\frac{d^2\sigma}{d\Omega d\omega'} \sim \frac{I(y^{1/2})}{y^{1/2}} \tag{36}$$

with

$$y = \frac{M_{j_1}M_{j_2}}{\mu(M_{j_1}+M_{j_2})} \frac{\omega' + \Omega_{j_1}(0) + \Omega_{j_2}(0)}{\Omega_{\mathrm{LO}}} \ .$$

The line shapes of the scattered lines are therefore intimately connected with the momentum dependence of the coupling functions. Figure 5 contains plots of Eq. (36) for several incident frequencies in the case of TO + LO scattering. Figure 6 shows the corresponding linewidths and shifts. Similar results hold for 2LO scattering. Most interesting is the strong dependence of line shapes due to phonon dispersion on incident frequencies. This allows one to differentiate in an experiment the constant intrinsic anharmonic linewidth from the linewidth due to phonon dispersion.

The symmetric shapes of the theoretical curves in Fig. 5 are typical for the Fröhlich interaction: The Fröhlich coupling first increases sharply with momentum, goes through a maximum, and then decreases slowly. Figure 6 shows that the line shift is large far away from the band edge and decreases dramatically if the incident frequency approaches the band edge. The linewidth is large for incident frequencies well below the band edge and becomes rather small in the electron-hole continuum. These predictions agree at least qualitatively with experimental observations in CdS.[20]

ACKNOWLEDGMENTS

The author thanks Professor M. Cardona and B. A. Weinstein for some discussions and for making available their experimental data prior to publication.

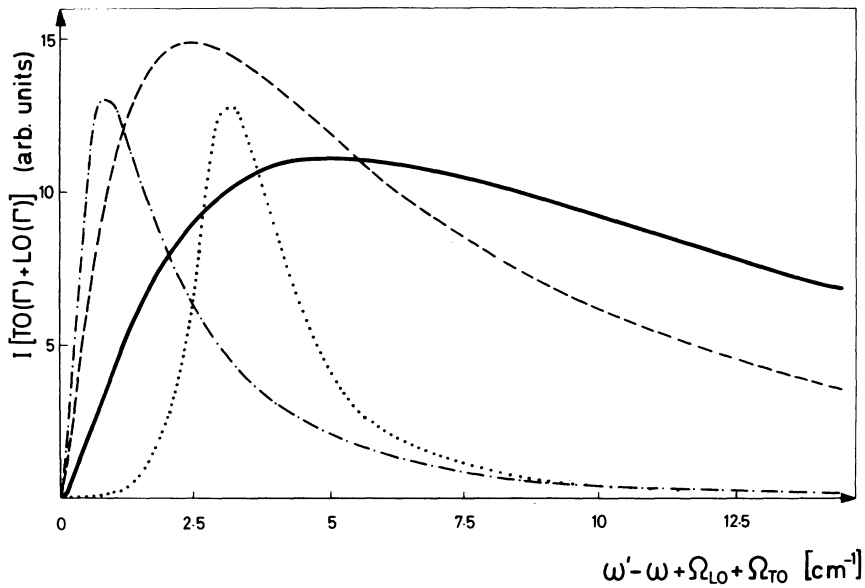

FIG. 5. ω' dependence of the differential cross section for TO(Γ) + LO(Γ) scattering for different incident frequencies: Straight line, $\hbar\omega = E_g - 3\hbar\Omega_{LO}$; dashed line, $\hbar\omega = E_g - \hbar\Omega_{LO}$; dot-dashed line, $\hbar\omega = E_g + \hbar\Omega_{LO}$; dotted line, $\hbar\omega = E_g + 3\hbar\Omega_{LO}$. The curves describe the line shapes of the scattered photons. We used the following phonon masses, taken from Ref. 19; $M_{TO}/m = \infty$, $M_{LO}/m = 720$; m is the free electron mass.

APPENDIX: DETERMINATION OF THE DEFORMATION POTENTIAL C BY A PSEUDOPOTENTIAL CALCULATION

We generalize in the following some formulas given in Ref. 13 to the case of GaP, where the pseudopotential has also an antisymmetric part. Restricting to plane waves with reciprocal lattice vectors $(2\pi/a_0)|\vec{G}| = 3$ or 4, the Γ_{15} valence bands are obtained by diagonalizing a 3×3 matrix. The associated basis vectors have the form

$$\Gamma_{15,X} = \alpha[111]_{\Gamma^{(1)}_{15,X}} + \beta[111]_{\Gamma^{(2)}_{15,X}} + \gamma[200]_{\Gamma_{15,X}} ,$$

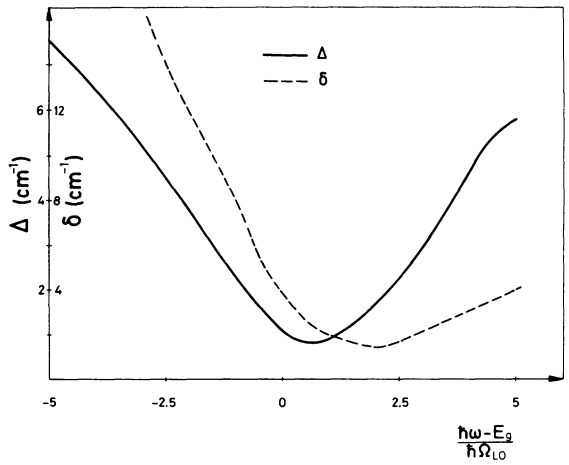

FIG. 6. Shift Δ and width δ of the line shape for TO(Γ) + LO(Γ) scattering using the same masses as in Fig. 5.

where, for instance, $[111]_{\Gamma^{(1)}_{15,X}}$ denotes the basis vector X of the first Γ_{15} representation in the space of the eight plane waves with wave vectors $(2\pi/a_0)|\vec{G}| = 3$. Using the pseudopotential values of Ref. 14 one obtains for GaP $\alpha = +0.637$, $\beta = -i0.324$, $\gamma = 0.699$.

The deformation potentials for optical phonons give the change in band energies due to the sublattice shift $\tau = (a_0/8)(1+\delta, 1+\delta, 1+\delta)$. For $\delta \neq 0$ the Γ_{15} representation splits into a Λ_1 and Λ_2 representation and

$$\bar{X} = \frac{1}{2^{1/2}}(X - Y)$$

can be taken as one of the two basis functions for the Λ_2 representation. Using the definitions of Ref. 13 the deformation constant d_0 is obtained from

$$d_0 = -(8/\sqrt{3})\langle \Gamma_{15,\bar{X}} | \frac{dV}{d\delta} | \Gamma_{15,\bar{X}} \rangle$$

$$= -4\pi/\sqrt{3}\,\{(|\alpha|^2 - |\beta|^2)(V_4^S - V_{12}^S)$$

$$+ \alpha\gamma\sqrt{2}(V_3^S - V_{11}^S) - \sqrt{2}i\beta\gamma(V_3^A - V_{11}^A)\}$$

$$= 26.3 \text{ eV} .$$

From that follows for our deformation potential C:

$$C/\hbar\Omega_{LO} = \frac{d_0}{2\hbar\Omega_{LO}}\left(\frac{\hbar a_0}{8\Omega_{TO}\mu a^3}\right)^{1/2} = 0.097 .$$

[1]B. Bendow, J. L. Birman, A. K. Ganguly, T. C. Damen, R. C. C. Leite, and J. F. Scott, Opt. Commun. 1, 267 (1970).
[2]B. Bendow, Phys. Rev. B 2, 5051 (1970).
[3]R. Martin, Phys. Rev. B 4, 3676 (1971).
[4]R. Zeyher, C. S. Ting, and J. L. Birman (unpublished).
[5]A. K. Ganguly and J. L. Birman, Phys. Rev. 162, 806 (1967).
[6]B. Bendow, Phys. Rev. B 4, 552 (1971).
[7]B. A. Weinstein and M. Cardona, Phys. Rev. B 8, 2795 (1973).
[8]D. C. Hamilton, Phys. Rev. 188, 1221 (1969).
[9]R. M. Martin and C. M. Verma, Phys. Rev. Lett. 26, 1241 (1971).
[10]R. Zeyher (unpublished).
[11]P. Y. Yu, Y. R. Shen, Y. Petroff, and L. M. Falikov, Phys. Rev. Lett. 30, 283 (1973).
[12]W. Dreybrodt, W. Richter, and M. Cardona, Solid State Commun. 11, 1127 (1972).
[13]H. Fröhlich, in *Polarons and Excitons*, edited by C. G. Kuper and G. D. Whitfield (Oliver and Boyd, Edinburgh, 1962).
[14]R. A. Cowley, in *The Raman Effect*, edited by A. Anderson (M. Dekker, New York, 1971) Vol. 1.
[15]M. Cardona, in *Atomic Structure and Properties of Solids* (Academic, New York, 1972).
[16]M. L. Cohen and T. K. Bergstresser, Phys. Rev. 141, 789 (1966).
[17]O. Madelung, *Physics of III-V Compounds* (Wiley, New York, 1964), pp. 100 and 353.
[18]A. Mooradian and G. B. Wright, Solid State Commun. 4, 431 (1966).
[19]J. L. Yarnell, J. L. Warren, R. G. Wenzel, and P. J. Dean, *Inelastic Neutron Scattering* (IAEA, Vienna, 1968), Vol. I, p. 30.
[20]T. C. Damen, R. C. C. Leite, and J. Shah, *Proceedings of the Tenth International Conference on the Physics of Semiconductors, Cambridge, Mass.*, 1970 (U. S. Atomic Energy Commission, Washington, D. C., 1970), p. 735.